

THERMODYNAMIC BENCHMARKING OF sCO₂ ALLAM CYCLE AGAINST ALTERNATIVE OXY-FUEL CYCLES: A COMPARATIVE ANALYSIS

Ihtishamul Haq*

IET, Vienna University of Technology
Vienna, Austria

Email: Ihtishamul.haq@tuwien.ac.at

Andreas Werner

IET, Vienna University of Technology
Vienna, Austria

Markus Haider

IET, Vienna University of Technology
Vienna, Austria

Abstract

To explore the potential of oxy-fuel technology, a detailed thermodynamic analysis is performed for four different oxy-fuel combustion cycles: the SCOC-CC, Matiant cycle, S-Graz cycle, and Allam cycle. Based on the literature data, these thermal cycles are modeled and simulated at full load using commercial software Aspen Plus with the same input and boundary conditions. The results show that the Allam cycle and S-Graz reach the highest net energy efficiency with 56.04% and 53.19%, respectively. The Matiant cycle and SCOC-CC have lower efficiencies at 50.02% and 45.23%, respectively. The exergy efficiency is also higher for the Allam cycle (52.87%) and the S-Graz cycle (50.18%). Moreover, the CCS efficiency penalty is comparatively higher for S-Graz, SCOC-CC, and Matiant, with 3.88%, 1.78%, and 1.70%, respectively. This is primarily because of the lower condenser pressure than the Allam cycle, which has a penalty of 0.42%. The ASU efficiency penalty is consistent at 10.31% for all cycles due to the same delivery pressure, flow rate, and oxygen purity. However, in the Allam cycle, it is marginally higher by 0.71 ppt due to an extra oxygen compressor. The results also indicate that the turbine main parameters, such as inlet temperature, inlet pressure, outlet pressure, and condenser pressure, strongly influence the system overall performance. The Allam cycle generally stands out for its high thermal efficiency and simple configuration.

1. Introduction

Rapid climate variations are severe challenges today due to the increase in greenhouse gas (GHG) emissions, particularly carbon dioxide (CO₂), which is the primary reason for global warming [1]. According to statistics from the European Commission Joint Research Centre (JRC) report, CO₂ emissions from burning fossil fuels increased by 67% between 1990 and 2021 [2]. The continuous rise in CO₂ emissions, mainly from power industry, transportation, and industrial processes, has led to unprecedented environmental shifts. These changes include increasing global temperature, loss of glaciers, and frequent and severe weather conditions, which pose significant threats to ecosystems, economies, and human life. To restrict the increase in global temperatures to

1.5°C above pre-industrial levels, as stated in the Paris Agreement, substantial reductions in CO₂ emissions are essential [3]. CO₂ capture and storage (CCS) technologies must be implemented to address this challenge and maintain environmental sustainability amid growing populations and rising energy consumption. The Center for Climate and Energy Solutions (C2ES) estimates that by 2050, CCS could be responsible for achieving 14% of the total greenhouse gas emissions needed to meet global climate goals [4].

Carbon capture-based technologies play an essential role in achieving a reduction of harmful CO₂ emissions. Currently, three prominent technologies exist for CCS, including pre-combustion, post-combustion, and oxy-fuel combustion [5]. In the pre-combustion process, fuel is converted into syngas (CO/H₂) by partial oxidation in the presence of oxygen or steam, which undergoes a water-gas shift reaction to make hydrogen-rich gas [6]. This technology consumes less energy and offers a high separation efficiency of 90% [7]. In post-combustion technology, CO₂ is captured from the exhaust of flue gases after fuel combustion by using some chemical solvents such as amine (MEA) [8]. This process is already implemented in power plants. However, this technology captures CO₂ with high energy consumption and cost [9]. In the last category for CO₂ capture, fuel is burned in an oxy-fuel combustion process with almost pure oxygen, producing CO₂-enriched flue gas consisting mainly of water, and CO₂, which can be easily separated and stored after the condensation process [10]. This technology is used in metallurgical industries, coal-fired power plants and also considered for cement plants [11]. Oxy-fuel combustion technology is considered a promising approach for decreasing emissions of CO₂ from fossil fuel-based power plants due to complete combustion process and its inherent potential to capture carbon nearly 100% [12]. The general block diagram of oxy-fuel combustion technology is shown in Figure 1. In this process flow chart, high-purity oxygen from the Air Separation Unit (ASU) is used to combust the fuel in the chamber. The generated thermal energy is converted into mechanical power by expanding hot combustion products in the turbine within the

power generation unit. Waste heat is recovered in order to improve the system's overall performance. Since the flue gas in the oxy-combustion cycle primarily comprises CO₂ and water, liquid water can be easily removed from the gas after condensation. The separated CO₂ can be stored, with a portion recycled to regulate the combustor temperature. In recent decades, several configurations of oxy-fuel power cycles have been suggested. Among these, four oxy-fuel combustion cycles that have demonstrated significant potential in earlier studies are the SCOC-CC, MATIANT cycle, S-Graz cycle, and NET power cycle (Allam cycle) [13, 14]. In the SCOC-CC, MATIANT cycle, and Allam cycle, CO₂ used as the recirculated working fluid, while in the Graz power cycle, steam is recycled to control combustion temperature.

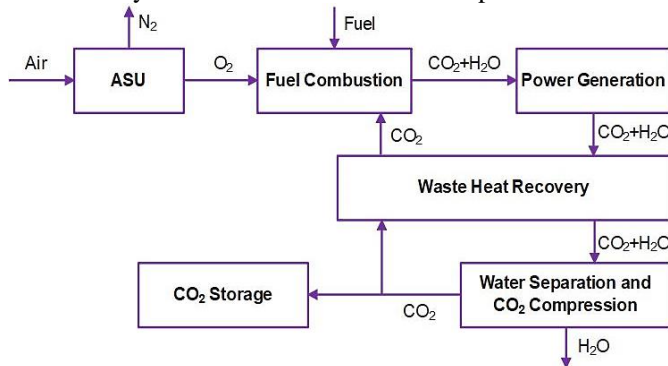


Figure 1. General diagram of the oxy-combustion power generation system

Different oxy-combustion cycles have been studied by L. Mancuso et al. [13], they calculated the net energy efficiency for each cycle, but did not investigate the detailed efficiency penalty of ASU and CCS. Moreover, the impact of critical parameters in each cycle on overall performance was not thoroughly addressed. Similarly, in another work on the water cycle, Graz cycle, and Matiant cycle, a detailed ASU and CCS energy consumption model was not developed, highlighting the need for further analysis [14].

This work conducts a comprehensive thermodynamic analysis of four different oxy-fuel combustion cycles. The detailed process flow diagram is demonstrated for each cycle, using components modeling, including an oxy-turbine with cooling, combustor, recuperator, and compressors. In SCOC-CC and S-Graz, the simple stage-by-stage model is used for turbine cooling [15], and for the Allam cycle turbine cooling, the El-Masri continuous expansion model is considered [16]. For CO₂ capture and transport, a multi-stage compression with intercooling technique is introduced in each cycle to investigate its impact on the overall performance. Similarly, the effect of the ASU technology with the same delivery pressure and oxygen purity is considered in the analysis. These power cycles are simulated using Aspen Plus with the same input conditions and carbon capture pressure. The overall performance of each cycle is assessed by net energy and exergy efficiency. Moreover, the study explored the impact of critical variables for the turbine such as inlet pressure, exit pressure and inlet temperature over a wide range on system performance. These

findings will offer valuable insights for choosing an appropriate cycle with significant potential and will serve as a basis for future improvements in each cycle layout.

2. Description of the oxy-fuel cycles and ASU

2.1 SCOC-CC

The SCOC-CC was introduced and published by O. Bolland and S. Saether in 1992 [17]. Figure 2 illustrates the process diagram of the SCOC-CC with a three-pressure heat recovery steam generator (HRSG). The SCOC-CC features a simple design comprising a Brayton cycle (comb, HTT, Cond2, Sep, and CC) alongside a standard Rankine cycle (HPT, MPT, LPT, HPP, MPP, LPP, Cond1, and HRSG). The natural gas is burned with excess oxygen to achieve a complete combustion.

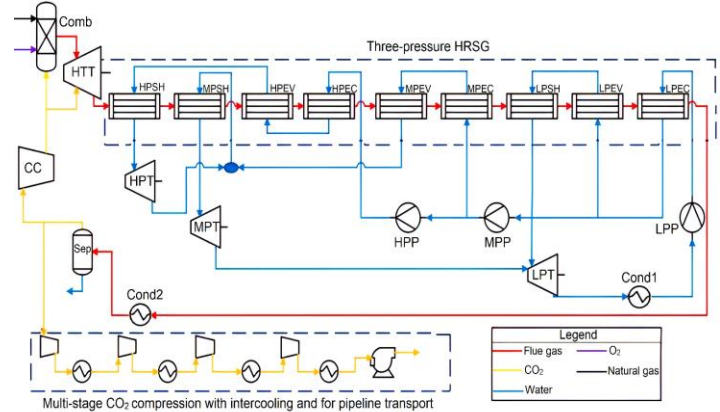


Figure 2. Process flow diagram of SCOC-CC with three-pressure regenerator and intercooled CO₂ compression. The combustion flue gas in SCOC-CC consists of CO₂ (92.5%), H₂O (7.1%), O₂ (0.3%), and N₂ (0.1%) by mass fraction [18]. The high-temperature turbine (HTT) operates at maximum temperature and pressure of 1400 °C and 40 bar, respectively [13]. In the bottom cycle, three different turbines, HPP, MPP, and LPP, operate at 120 bar, 27 bar, and 4 bar, respectively, and are linked to the generator by a single shaft. The super-heated steam enters HPT at 120 bar and 570 °C, the expanded working fluid at 27 bar mixed with saturated vapor from MPEV, is reheated to 570 °C in MPSH and then enters MPT, which expands to 4 bar. The exhaust steam from the LPSH and sent to the LPT at 4 bar and 284 °C. Following the expansion in the LPT, the working fluid is directed to the condenser (Cond1) at 0.04 bar and 32 °C. The separated CO₂ is split up into two streams: one portion is compressed in the compressor CC at 40 bar and used to adjust the combustion temperature and to cool the turbine blades, while the remaining portion is compressed using multi-stage compression and transported to the pipeline at 120 bar.

2.2 Matiant cycle

The concept of the Matiant cycle was invented by the two scientists in 1997 and titled in honor of their names, P. Mathieu and E. Iantovski [19]. The process diagram of the cycle consists of two combustion chambers (comb1 and comb2) and three turbines (HPT, MPT, and LPT), as shown in Figure 3, which utilize CO₂ to regulate the combustion temperature in

Comb1[20]. The chilled CO₂ undergoes a multi-stage

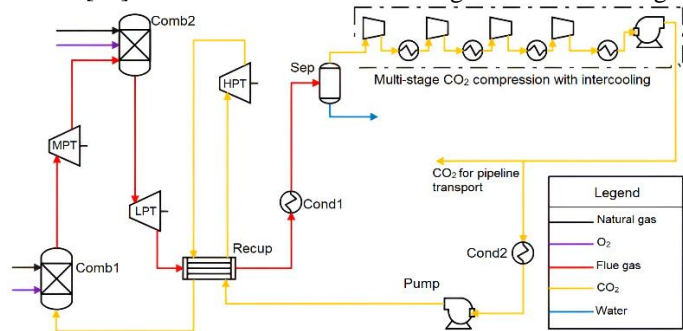


Figure 3. Process flow diagram of Matiant cycle with intercooled CO₂ compression

compression with intercooling and is delivered at 120 bar under supercritical conditions, and then some portion of the compressed CO₂ is transported to the pipeline. At the same time, the remaining is pumped to the recuperator at 300 bar, after which it is heated to approximately 600 °C within the recuperator [21]. The high-pressure stream expands to 40 bar in the HPT before returning to the recuperator for further heating. Next, it proceeds into the combustor (Comb1) to maintain the combustion temperature at 1300 °C, and the resulting flue gas undergoes expansion within the MP turbine at 40 bar. Subsequently, a reheating combustion chamber (Comb2) raises the flue gas temperature to 1300 °C, allowing it to expand further within the LP turbine to 1 bar. The thermal efficiency range for the Matiant power cycle is 45-49% [21].

2.3 S-Graz cycle

The concept of the Graz cycle was designed by Herbert Jericha in 1985, at the Graz University of Technology, and a new version with a high steam (S-Graz) presented at the ASME Turbo Expo conference in 2004 [22]. The detailed process diagram of S-Graz is illustrated in Figure 4. This cycle is composed of a Brayton cycle (Comb, HTT, LPT and compressors C1/C2) and a subcritical Rankine cycle (HPT, HRSG, Pump, and condenser). The fuel undergoes combustion with excess oxygen, and the hot flue gas stream at 1400 °C and 40 bar is expanded within the HTT to atmospheric pressure. The combustion product includes 74% water, 25.3% CO₂, 0.5% oxygen, and 0.2% nitrogen by mass [22]. The energy is recovered from the flue gas in a HRSG (SH, Cond2, EV, and PH) to produce steam at 570 °C [23]. The high-pressure steam at 180 bar is expanded to 40 bar in the HPT. The HPT exit stream is distributed into two separate flows. The flow with the highest proportion is used to regulate the combustion temperature, and the remaining flow is employed as a cooling flow for the HTT. The flue gas leaving the evaporator (EV) is split up into two separate streams. One stream is directed to a multi-stage inter-cooled compressor (C1/C2) after passing through the pre-heater (PH), and the exit temperature of compressor C2 is kept below 600 °C to insure sufficient creep resistance of the materials [23]. The other stream runs LPT, expanding to a vacuum pressure of 0.04 bar. The separated CO₂ undergoes compression across multiple stages before being transported to the pipeline at a pressure of 120 bar. The thermal

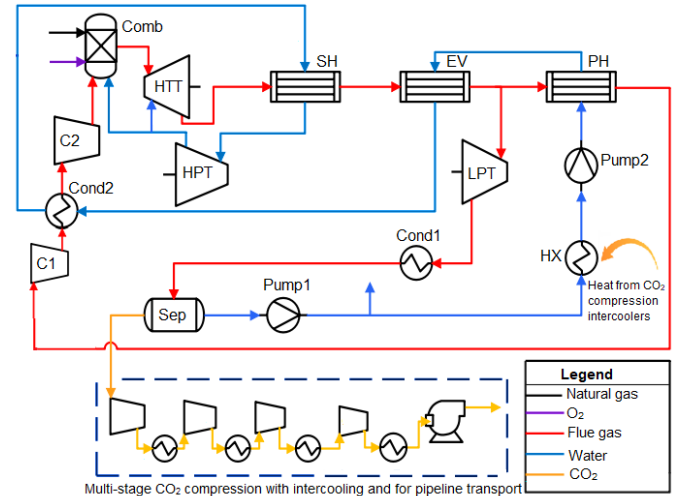


Figure 4. Process flow diagram of S-Graz cycle with intercooled CO₂ compression

efficiency for the Graz power cycle was computed at 53.12% [24].

2.4 Allam cycle

The Allam cycle was introduced by Rodney John Allam in 2010 [25]. Its detailed process schematic with CCS is illustrated in Figure 5. Net Power, the developer of the Allam cycle 50 MWth scale plant fired by natural gas, has already tested the facility in La Porte, Texas [26]. The natural gas and high-pressure oxygen at 300 bar are combined and burned in the combustor. The composition of the working fluid in the Allam cycle consists of approximately 96% CO₂ and 3% steam [23]. The flue gas leaving the combustion chamber at 300 bar and 1150 °C is expanded in the supercritical CO₂ turbine to 34 bar and 745 °C. The flue gas is cooled in the condenser to near-critical condition after passing through a high-temperature recuperator. At this stage, water content is separated from flue gas in the separator, and CO₂ is compressed using multi-stage

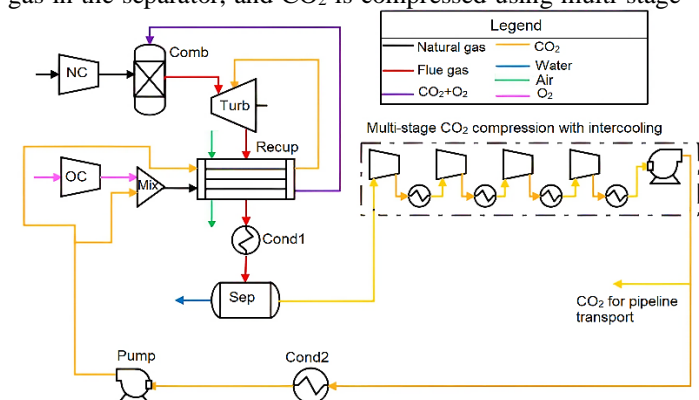


Figure 5. Process flow diagram of the Allam cycle with intercooled CO₂ compression

compression to a pressure of 120 bar. Some of the CO₂ is transported to the pipeline for storage, while the remaining CO₂ is cooled in the pre-cooler and increased its pressure to 300 bar. Further, high-pressure cooled CO₂ is divided into two streams. One mixed with oxygen before entering the recuperator to

control combustion temperature, and the other with a small amount is used to cool the turbine. The highest energy efficiency reported for the Allam cycle is 55.1% [13].

2.5 Air Separation Unit

The ASU system is modeled based on cryogenic techniques for atmospheric air. The composition of air by volumetric analysis includes nitrogen (78.1%), oxygen (21%), and argon (0.9%). The ASU is modeled with a high-pressure column (HPC) and low-pressure column (LPC) with stages 20 and 29, respectively, as shown in Figure 6. Initially, the air is compressed to 5.5 bar in the main air compressor (MAC); the liquid oxygen in the heat exchanger recovers energy from the compressed air. Since the process is an air cryogenic process, the air temperature is dropped to -180 °C in the condenser. Then, the air flow splits into two streams; a significant portion of the air is introduced into the lower section of the HPC at a temperature slightly above the condensation point. Due to nitrogen higher vapor pressure than oxygen and argon at the same temperature, nitrogen accumulates at the top of the HPC, while oxygen-rich liquid with a purity of 35% accumulates at the bottom. Both streams are further cooled, and the pure nitrogen is then introduced to the top of the LPC as reflux to cool the rising gases. Meanwhile, the purified liquid oxygen from HPC is introduced in the middle of the LPC after its pressure is reduced from 5.5 bar to 1.35 bar. After the distillation process, the liquid oxygen is pressurized using a pump. The oxygen is supplied to the combustor with a purity of 99% under a pressure of 120 bar and temperature of 15 °C. The oxygen flow rate is set with 3% excess to achieve a complete combustion and maintain flame steadiness.

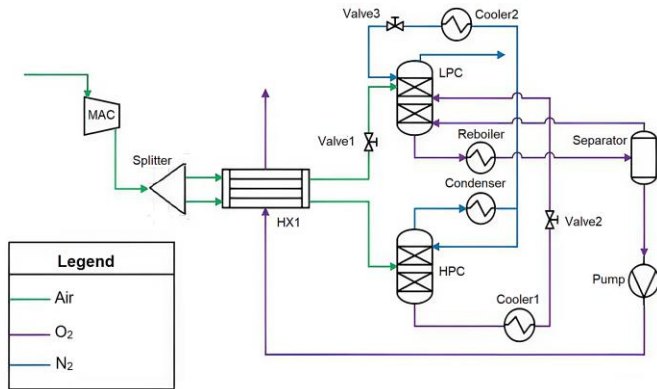


Figure 6. ASU model with two columns

3. Process modeling and assumptions

The oxy-fuel cycles, including SCOC-CC, Matiant cycle, Graz cycle, and Allam power cycle, are modeled and simulated using a simulation software called ASPEN PLUS. RGibbs reactor is used in Aspen Plus simulation in each cycle as a combustor to model chemical and phase equilibrium, which relies on minimizing Gibbs free energy. This work employs the Peng-Robinson EOS as the base method for all modeling aspects, including the primary cycle, ASU, and CCS. The isentropic, mechanical, and hydraulic efficiencies assumed for the components in each cycle are summarized in Table 1. The chemical composition and thermodynamic characteristics of

natural gas as a fuel are illustrated in Table 2. Oxygen is supplied from the ASU with 99% purity, but ASU is considered outside the simulation model in all cases. The total input heat from the fuel is set at 768 MW, combusted in excess oxygen (3%). The simulation of each cycle is established on the following assumptions:

- The ambient pressure and temperature are 1 bar and 25 °C, as standard condition.
- The main components, including compressors, pumps, valves, and turbines, are adiabatically modeled.
- Heat transfer and pressure losses in the pipelines are neglected.

Table 1. Components assumed efficiencies for the simulation model

Component	Parameter	Value
Turbine	Isentropic efficiency	0.89
	Mechanical efficiency	0.98
Water pump	Hydraulic efficiency	0.85
	CO ₂ compressor	Isentropic efficiency
CO ₂ pump	Hydraulic efficiency	0.85
	Oxygen compressor	Isentropic efficiency
Natural gas compressor	Polytropic efficiency	0.85
Flue gas compressor	Isentropic efficiency	0.88
Generator	Electric efficiency	0.99

4. Thermodynamic analysis and evaluation criteria

The thermal modeling of the cycle is established by applying mass, energy, and exergy conservation principles on the control volume of each element. The First Law of Thermodynamics evaluates the energy quantity in a system. The details of a system's actual performance can be examined by its useful energy, which is called the exergy of the system. The system exergy is the total work obtained due to the system's interaction with its environment, considering the impact of irreversibility in the process. The cumulative flow exergy of a system is the total of physical, kinetic, potential, and chemical exergies. Physical exergy exists because of the differences in temperature and pressure between the system and its surroundings. Chemical exergy results from variations in the chemical composition of the system occurring in the combustion chamber compared to the environment. Kinetic exergy is attributed to the system velocity relative to the dead state, while potential exergy is linked to the system's elevation relative to the environment.

First, we evaluated the mass balance at steady state using Eq. 1 [27]:

$$\sum \dot{m}_{in} = \sum \dot{m}_{out} \quad (1)$$

The energy balance of the system was investigated at steady state conditions using Eq. 2 [27]:

$$\dot{Q}_{in} + \dot{W}_{in} + \sum \dot{m}_{in} h_{in} = \dot{Q}_{out} + \dot{W}_{out} + \sum \dot{m}_{out} h_{out} \quad (2)$$

The exergy balance and exergy destruction for the control volume system at steady state conditions were estimated using Eq. 3 [28]:

$$\dot{E}_{in} - \dot{E}_{out} - \dot{E}_D = 0 \quad (3)$$

Where \dot{E} represents the exergy rate, and which can be transferred by heat $\dot{E}_{heat} = \int (1 - \frac{T_0}{T}) \delta \dot{Q}$, by work $\dot{E}_{work} = \dot{W}$, by mass flow $\dot{E}_{flow} = \dot{m}\psi$ and $\dot{E}_D = T_0 \dot{S}_{gen} \geq 0$ represents the exergy destruction rate.

Table 2. Thermodynamics properties and volumetric composition of natural gas [13, 29]

Natural gas volumetric analysis	Value (%)
Methane	89
Ethane	7
Propane	1
Butane	0.1
Pentane	0.01
CO ₂	2
N ₂	0.89
Molecular weight (kg/kmol)	18
Temperature (°C)	15
Pressure (bar)	70
Lower heating value (LHV) (kJ/kg)	46502

A system cumulative flow exergy (ψ) can be expressed as in Eq. 4 [30]:

$$\psi = e^{ph} + e^{ch} + e^{ke} + e^{pt} \quad (4)$$

Eq. 4 can be reformulated, as shown in Eq. 5, by neglecting kinetic and potential exergy:

$$\psi = e^{ph} + e^{ch} \quad (5)$$

The physical exergy rate of the system was determined using Eq. 6:

$$\dot{E}_{ph} = \dot{m}e^{ph} \quad (6)$$

Where e_{ph} is the specific physical exergy, and it was determined in terms of specific heat c_p by Eq.7 [31]:

$$e^{ph} = c_p \left((T - T_0) - T_0 \ln \frac{T}{T_0} \right) + \frac{k-1}{k} c_p T_0 \ln \frac{P}{P_0} \quad (7)$$

The chemical exergy rate of the system was determined using Eq. 8:

$$\dot{E}_{ch} = \dot{m}e^{ch} \quad (8)$$

Where the chemical-specific exergy e^{ch} of gas mixture was analyzed using Eq. 9 [32]:

$$e^{ch} = \sum x_k e_k^{ch} + RT_0 \sum x_k \ln x_k \quad (9)$$

Where x_k represents the mole fraction of element k, e_k^{ch} represents the specific standard chemical exergy of element k, as shown in Table 3, and R represents the molar gas constant.

The overall energy efficiency of thermodynamics can be defined as the ratio of net power output to the total input energy. In comparison, the overall exergetic efficiency of thermodynamics can be defined as the ratio of network output to the total fuel input exergy. Both efficiencies for each system are computed using Eq. 10 and Eq. 11, respectively [33]:

$$\eta_{th,overall} = \frac{\dot{W}_{net}}{\dot{Q}_{in}} \quad (10)$$

Where $\dot{W}_{net} = \sum \dot{W}_{turb} - \sum \dot{W}_{con}$, \dot{W}_{turb} is the total power produced by the turbines, and \dot{W}_{con} is the total power consumed by the ASU, pumps, compressors, and CCS.

$\dot{Q}_{in} = \dot{m}_{fuel} LHV_{fuel}$ is the total heat input by the fuel.

Electric efficiency can be calculated as: $\eta_{ele} = \varphi \times \eta_{th}$
Where φ is generator efficiency

$$\eta_{ex,overall} = \frac{\dot{W}_{net}}{\dot{E}_{in,fuel}} \quad (11)$$

Where, $\dot{E}_{in,fuel}$ represents the rate of fuel exergy input.

$$\dot{E}_{in,fuel} = \dot{m}_{Fuel} e_{Fuel}$$

The specific exergy flow of the fuel can be calculated by using Eq. 12 [34]:

$$\xi = \frac{e_{fuel}}{LHV_{fuel}} \quad (12)$$

Where ξ is the ratio of fuel-specific exergy to the lower heating value of the fuel; generally, the value of $\xi = 1.06$ is considered for natural gas [35].

Table 3. Standard chemical exergy values of the gasses at reference state conditions ($T_0 = 25$ °C and $P_0 = 1$ bar) [36, 37]

Species	e_k^{ch} (kJ/kmole)
CO	275100
CO ₂	19860
H ₂ O liquid	900
H ₂ O vapor	9500
H ₂	236100
O ₂	3970
Argon	11690
CH ₄	831650
C ₂ H ₆	1495840
C ₃ H ₈	2154000
C ₄ H ₁₀	2805800
C ₅ H ₁₂	3461300

5. Model validation

The simulation results for each cycle considered in this study are validated with the literature results [13, 18, 21, 23, 29, 38]. The power balance is drawn in Table 4 for SCOC-CC, Matiant cycle, S-Graz cycle, and Allam cycle, respectively. The simulation outcomes are consistent with those in the reference studies, demonstrating the models accuracy in this research.

6. Results and discussion

The four oxy-fuel combustion cycles, including SCOC-CC, Matiant cycle, S-Graz cycle, and Allam cycle, are analyzed and compared with the same input conditions. These power cycles are modeled and simulated based on their design operating values using Aspen Plus.

The power balance flow sheet with detailed energy consumption for each cycle is demonstrated in Table 4. The bar chart in Figure 7 compares the power outputs, energy consumption by the ASU, and recycle flow compressors of these power generation cycles. Regarding gross power output, S-Graz leads with 729.62 MW, followed by SCOC-CC with 681.86 MW, benefiting from the combined cycle. The Allam cycle achieved the maximum net electric power out of 426.20 MW primarily due to its lower power consumption for recycling flow. The recycle flow power consumption is almost one-third of the total power output in the SCOC-CC and S-Graz cycle, mainly due to flue gas compression and high flow rates. In the Allam cycle, the high operating pressure necessitates

using two additional compressors for natural gas and oxygen compression to raise its pressure to 300 bar.

In case of CCS power consumption, the efficiency penalty (3.88%) is relatively high for the S-Graz cycle due to the shallow pressure of the condenser as compared to the SCOC-CC and Matiant cycle, with efficiency penalty 1.78% and 1.70%, respectively as shown in Figure 8. In contrast, the Allam cycle experiences a lower penalty of 0.42% due to its high turbine outlet pressure, which minimizes the power needed

Table 4. Performance comparison of the oxyfuel combustion cycles

	SCOC -CC	Matiant cycle	S-Graz cycle	Allam cycle
Thermal energy input (LHV) [MW]	768.21	768.21	768.21	768.21
Turbine power output [MW]	681.86	643.53	729.62	609.78
Recycle flow power consumption [MW]	241.55	166.11	212.01	87.17
ASU power consumption [MW]	79.21	79.21	79.21	79.21
OC power consumption [MW]				5.61
NG compressor power consumption [MW]				4.04
CCS power consumption [MW]	13.67	13.97	29.81	3.26
Net mechanical power out [MW]	347.44	384.24	408.59	430.50
Energy efficiency (LHV) [%]	45.23	50.02	53.19	56.04
Net electric power output [MW]	343.97	380.40	404.51	426.20
Net electric efficiency [%]	44.77	49.52	52.66	55.48

to compress CO₂ to 120 bar. The ASU efficiency penalty for the Allam cycle (11.04%) is slightly higher because of the additional oxygen compressor. In comparison, other cycles experience an equal penalty (10.31%) due to the same delivery pressure, flow rate, and oxygen purity. Overall, the Allam cycle achieves the highest net energy efficiency at 56.04%, followed by the S-Graz cycle at 53.19%. The Matiant cycle and SCOC-CC exhibit lower efficiency with 50.02% and 45.23%, respectively primarily attributed to the high energy usage of the recycle flow compressors and pumps, as computed in Table 4. In terms of cycle configuration, the Allam cycle features a straightforward design consisting of one loop with a single combustor, turbine, and recuperator, in contrast to other cycles that involve multiple loops and turbines. This simplicity may lead to reduced operational complexity and lower costs. However, the recuperator in the Allam cycle is a considerably more complex component due to higher pressure differentials and elevated inlet temperature.

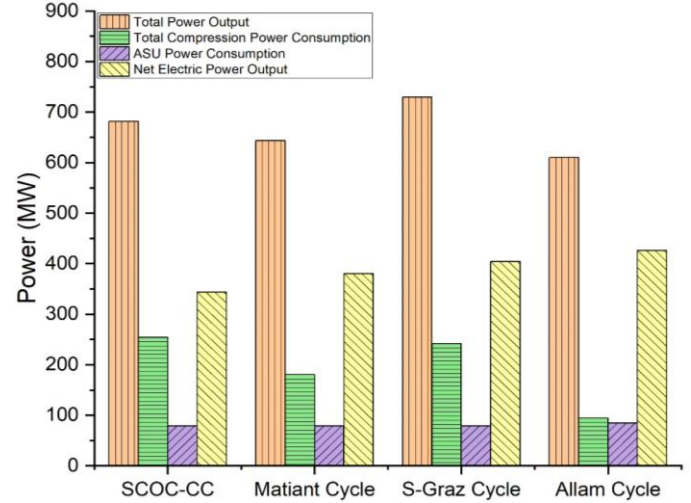


Figure 7. Power output and energy consumption comparison of SCOC-CC, Matiant, S-Graz, and Allam cycle

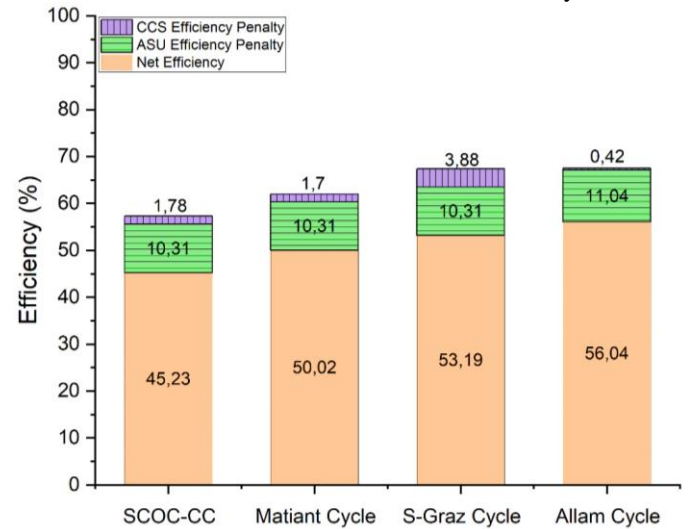


Figure 8. Efficiency comparison of SCOC-CC, Matiant, S-Graz, and Allam cycle with ASU and CCS penalty

7. Sensitivity analysis

In this study, the impact of the turbine key parameters such as turbine inlet temperature, turbine inlet pressure, and condenser pressure, on the overall performance are examined.

7.1 Effect of turbine inlet temperature

The turbine inlet temperature is a critical parameter that can significantly affect the system performance, as illustrated in Figure 9. For the Allam cycle, an optimal value is obtained for the turbine inlet temperature of 1150 °C, and the maximum energy and exergy efficiency achieved are 56.04% and 52.87%, respectively. Moreover, a reasonable temperature difference of 20 °C is found between the hot stream inlet and cold stream outlet at this value. Meanwhile, compression power consumption decreases due to reduced recycle mass flow rate. However, for the turbine inlet temperature above 1150 °C, the energy and exergy efficiency begin to decline. This reduction is mainly attributed to a decline in the mass flow at the turbine inlet, an increase in turbine cooling mass flow rate, and high

irreversibility within the recuperator as the turbine outlet temperature rises. In comparison, the S-Graz operates at a higher temperature, significantly enhancing thermal performance with an increased HTT inlet temperature. As the inlet temperature rises from 1200 °C to 1400 °C, the energy and exergy efficiency improve to 53.19% and 50.18%, respectively. This increase is primarily attributed to the higher average temperature of the heat input, which enhances the cycle thermal performance. Additionally, the reduction in mass flow rate at the HTT inlet decreases the compression power requirement, particularly for the recycled flue gas compressors. For the Matiant cycle, the HTT inlet temperature is varied between 1100 °C to 1400 °C, the maximum energy (50.02%) and exergy efficiency (47.18%) are obtained at optimum temperature of 1330 °C. However, beyond this temperature, the overall performance of the Matiant cycle decreases due to increased recycle flow consumption power and significant energy loss in the recuperator. The cycle complex configuration also contributes to higher irreversibilities, further limiting its performance. The performance of the SCOC-CC is linearly increased with HTT inlet temperature. As the temperature is increased by reducing the mass flow of cooling media, the power output and energy consumption are reduced, respectively, resulting in an increase in overall net power. The maximum energy and exergy efficiency are recorded 45.25% and 42.69%, respectively. Overall, these results emphasize the positive correlation between turbine inlet temperature and cycle performance, demonstrating the critical role of thermal management and optimizing efficiency.

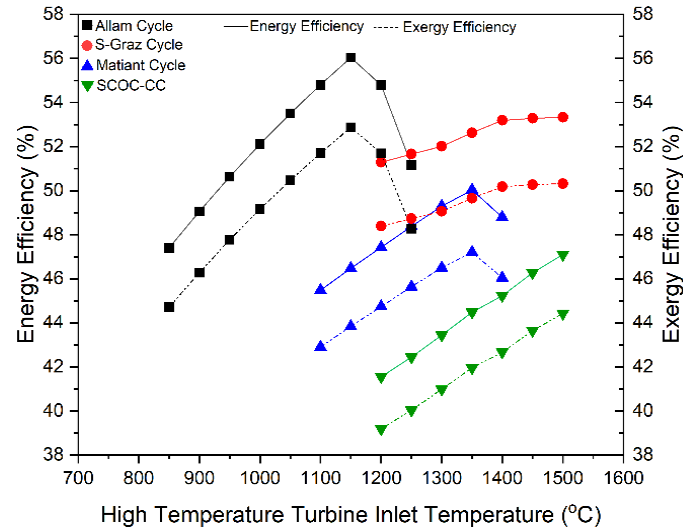


Figure 9. Impact of HTT inlet temperature on energy and exergy efficiency

7.2 Effect of turbine inlet pressure

The effect of turbine inlet pressure on each cycle performance is investigated as shown in Figure 10. The overall performance of the Allam cycle is enhanced by increasing the inlet pressure as a result of a reduction in turbine exit temperature, therefore, maximizing energy extraction from the hot flue gas. Moreover, at lower inlet pressure, the temperature at the recuperator inlet exceeded the threshold value since the

maximum allowable temperature is 760 °C due to material constraints [39]. As the pressure reached 300 bar, the energy and exergy efficiency improved by 2.1% and 1.98%, respectively, within the 240-300 bar range. However, beyond 300 bar, minimal changes in efficiencies are observed. In contrast, the HTT in the S-Graz cycle operates at a lower pressure. As the pressure increases, two different trends can be observed for the efficiencies. The energy and exergy efficiency improves significantly from approximately 51.36% and 48.45% at 30 bar, reaching a peak of nearly 53.19% and 50.18% at 40 bar. However, as the pressure surpasses 40 bar, both efficiencies decrease, returning to 52.17% and 49.22% respectively, at 50 bar. This indicates that although higher pressure initially enhances energy efficiency, there is an optimal point around 40 bar, beyond which the efficiency gains diminish. For the Matiant cycle, similar optimal operating pressure is witnessed. However, beyond 40 bar the system overall performance becomes stable. In the SCOC-CC, the HTT inlet pressure rises from 30 bar to 45 bar, the energy and exergy efficiency increased by 2.64% and 2.49%, respectively. Both efficiencies are linearly increased with increment in turbine pressure, but operating a turbine near or above 50 bar has several restrictions, including material limitations, operational complexity, and economic factors. In general, higher turbine inlet pressure enhances performance, each cycle exhibits an optimal pressure range beyond which efficiency improvements stabilize or decline due to thermodynamics and practical limitations.

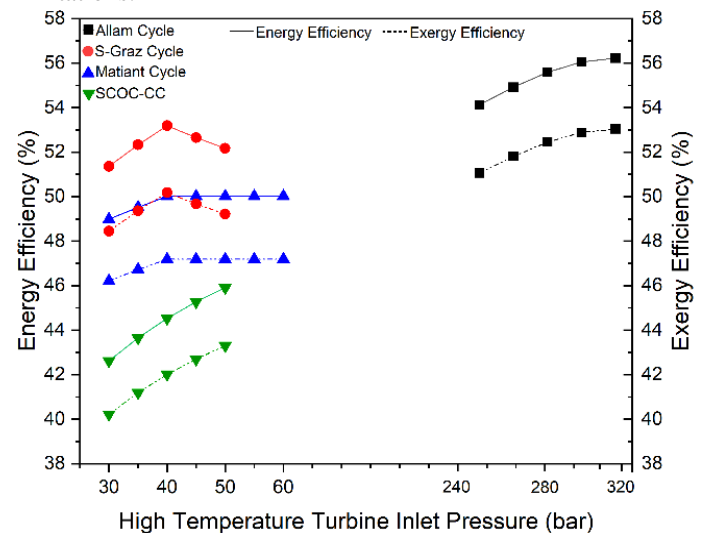


Figure 10. Impact of HTT inlet pressure on energy and exergy efficiency

7.3 Effect of condenser pressure

Figure 11 shows the impact of the condenser pressure on the cycle performance. In the Allam cycle, the turbine outlet pressure also enhances the performance. This improvement is primarily attributed to reduced CO₂ compression power due to the high outlet pressure. The maximum energy (56.04%) and exergy efficiency (52.87%) were observed at 34 bar. For turbine outlet pressures exceeding 34 bar, the turbine inlet temperature is reduced under 1150 °C to keep the turbine exit temperature

constant at 745 °C, which is the designated limit for the recuperator temperature. In the S-Graz cycle, the condenser operates under vacuum conditions, with maximum energy and exergy efficiency achieved at 0.04 bar. However, increasing the condenser pressure reduces the LPT power output. Although CO₂ compression power consumption decreases, the net power output declines, which negatively impacts the overall cycle performance. For the Matiant cycle, the effect of the condenser pressure between 0.5 bar and 1 bar on cycle performance is minimal. Initially, when the condenser pressure increases from 0.5 bar to 1 bar, the energy and exergy efficiency show a slight upward trend with a maximum value of 50.02% and 47.21%, respectively. However, beyond 1 bar, efficiencies decline sharply, falling below their peak values as pressure continues to increase. In the SCOC-CC, as condenser pressure grows from 1 to 1.5 bar, both efficiencies steadily decline. This indicates that a rise in condenser pressure leads to a slight reduction in the system power generation capacity. At a condenser pressure of 1 bar, the energy efficiency starts at 45.25% but decreases to 42.88% as the pressure rises to 1.5 bar. Similarly, the exergy efficiency decreases, falling from around 42.69% to 40.45%. This indicates that at a lower condenser pressure, the system performs more efficiently by maximizing energy extraction from the working fluid before condensation.

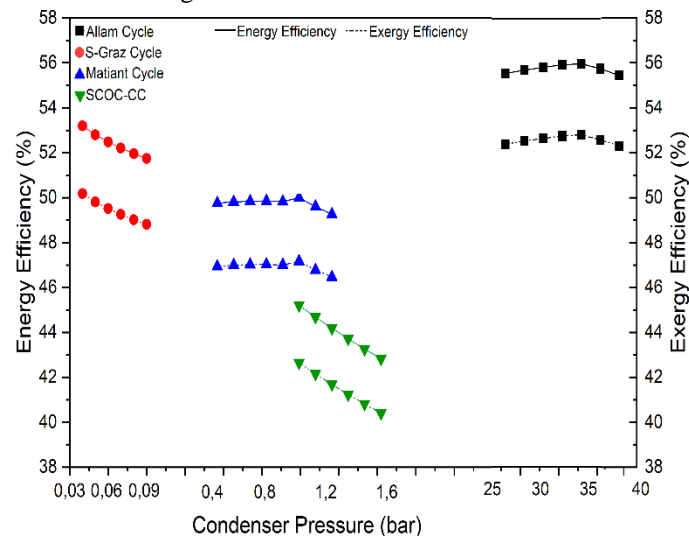


Figure 11. Impact of condenser pressure on energy and exergy efficiency

8. Conclusion

This study provides an in-depth thermodynamic analysis of four oxy-fuel combustion cycles: SCOC-CC, Matiant cycle, S-Graz cycle, and Allam cycle. The findings suggest that the Allam cycle reaches the highest net energy efficiency at 56.04%, with the S-Graz cycle at 53.19%. Conversely, the Matiant cycle and SCOC-CC have lower efficiencies at 50.02% and 45.23%, respectively. The efficiency penalty of the ASU in the Allam cycle is slightly higher due to the additional compressor. The Allam cycle achieved the highest net electric power output of 426.20 MW, mainly due to its low compression power consumption.

Further, based on sensitivity analysis, the following insights can be concluded for each cycle:

- In the SCOC-CC system, the influence of HTT inlet temperature is greater than that of inlet pressure, while the condenser pressure also has a considerable effect.
- In the Matiant power cycle, the HPT is sensitive to inlet pressure and temperature due to the supercritical nature of CO₂ as the working fluid. However, the impact of MPT inlet temperature and pressure is more significant on the overall performance, with optimal efficiency achieved at 1330 °C and 40 bar.
- In the case of the S-Graz cycle, similar to the SCOC-CC system, the HTT inlet temperature and pressure highly impact the system performance. Sensitivity analysis indicates that the optimal HTT inlet conditions are 40 bar and 1400 °C, with an optimal condenser pressure of 0.04 bar.
- In the Allam cycle, the maximum net energy and exergy efficiency is achieved at an optimum inlet and outlet pressure of 300 bar and 34 bar, respectively. Similarly, the performance improved considerably for the turbine inlet temperature 1150 °C.

Acknowledgment

This work is supported by the European Union Horizon Europe research and innovation programme through the project "Innovation in Supercritical CO₂ Power Generation Systems (ISOP)" (Grant Agreement No. 101073266).

Nomenclature

SCOC	Semi-closed oxy-combustion	<i>Greek letters</i>
-CC	combined cycle	ψ Flow exergy
ASME	American Society of Mechanical Engineers	η Efficiency
MEA	Mono-ethanolamine	ξ Specific
HTT	High temperature turbine	flow exergy
HPT	High pressure turbine	ratio
MPT	Medium pressure turbine	ψ Cumulative
LPT	Low pressure turbine	flow exergy
Sep	Separator	<i>Subscripts</i>
ASU	Air separation unit	D Destroy
Cond	Condenser	gen Generation
PH	Pre-heater	ex Exergy
SH	Super heater	ph Physical
EC	Economizer	ch Chemical
HPP	High pressure pump	th Thermal
MPP	Medium pressure pump	ele Electric
LPP	Low pressure pump	ke Kinetic
CC	Carbon-dioxide compressor	Pt Potential
MAC	Main air compressor	
Comb	Combustor	
Recup	Recuperator	
Turb	Turbine	
OC	Oxygen compressor	
NC	Natural gas compressor	
Mix	Mixer	
Exp	Expander	

References

- [1] J. Blamey, E. Anthony, J. Wang, and P. Fennell, "The calcium looping cycle for large-scale CO₂ capture," *Progress in Energy and Combustion Science*, vol. 36, pp. 260-279, 2010.
- [2] M. Crippa, D. Guizzardi, M. Banja, E. Solazzo, M. Muntean, E. Schaaf, *et al.*, "CO₂ emissions of all world countries," *JRC Science for Policy Report, European Commission, EUR*, vol. 31182, 2022.
- [3] B. Cointe and H. Guillemot, "A history of the 1.5° C target," *Wiley Interdisciplinary Reviews: Climate Change*, vol. 14, p. e824, 2023.
- [4] *Carbon capture*. Available: <https://www.c2es.org/content/carbon-capture/>
- [5] C. Wu, Q. Huang, Z. Xu, A. T. Sipra, N. Gao, L. P. de Souza Vandenberghe, *et al.*, "A comprehensive review of carbon capture science and technologies," *Carbon Capture Science & Technology*, vol. 11, p. 100178, 2024.
- [6] N. S. Sifat and Y. Haseli, "A critical review of CO₂ capture technologies and prospects for clean power generation," *Energies*, vol. 12, p. 4143, 2019.
- [7] W. Hua, Y. Sha, X. Zhang, and H. Cao, "Research progress of carbon capture and storage (CCS) technology based on the shipping industry," *Ocean Engineering*, vol. 281, p. 114929, 2023.
- [8] M. Asif, M. Suleman, I. Haq, and S. A. Jamal, "Post-combustion CO₂ capture with chemical absorption and hybrid system: current status and challenges," *Greenhouse Gases: Science and Technology*, vol. 8, pp. 998-1031, 2018.
- [9] S. Budinis, S. Krevor, N. Mac Dowell, N. Brandon, and A. Hawkes, "An assessment of CCS costs, barriers and potential," *Energy strategy reviews*, vol. 22, pp. 61-81, 2018.
- [10] L. Zheng, *Oxy-fuel combustion for power generation and carbon dioxide (CO₂) capture*: Elsevier, 2011.
- [11] Z. Zhang, X. Li, C. Luo, L. Zhang, Y. Xu, Y. Wu, *et al.*, "Investigation on the thermodynamic calculation of a 35 MWth oxy-fuel combustion coal-fired boiler," *International Journal of Greenhouse Gas Control*, vol. 71, pp. 36-45, 2018.
- [12] S. Yadav and S. Mondal, "A review on the progress and prospects of oxy-fuel carbon capture and sequestration (CCS) technology," *Fuel*, vol. 308, p. 122057, 2022.
- [13] L. Mancuso, N. Ferrari, P. Chiesa, E. Martelli, and M. Romano, "Oxy-combustion turbine power plants," *IEAGHG report*, vol. 5, 2015.
- [14] O. Bolland, H. M. Kvamsdal, and J. C. Boden, "A thermodynamic comparison of the oxy-fuel power cycles water-cycle, graz-cycle and matiant-cycle," in *Power generation and sustainable development (Liège, 8-9 October 2001)*, 2001, pp. 293-298.
- [15] K. Jordal, O. Bolland, and A. Klång, "Aspects of cooled gas turbine modeling for the semi-closed O₂/CO₂ cycle with CO₂ capture," *J. Eng. Gas Turbines Power*, vol. 126, pp. 507-515, 2004.
- [16] M. El-Masri, "On thermodynamics of gas-turbine cycles: Part 2—a model for expansion in cooled turbines," 1986.
- [17] O. Bolland and S. Saether, "New concepts for natural gas fired power plants which simplify the recovery of carbon dioxide," *Energy Conversion and Management*, vol. 33, pp. 467-475, 1992.
- [18] W. Sanz, H. Jericha, B. Bauer, and E. Göttlich, "Qualitative and quantitative comparison of two promising oxy-fuel power cycles for CO₂ capture," 2008.
- [19] P. Mathieu and R. Nihart, "Zero emission MATIANT cycle," in *Turbo Expo: Power for Land, Sea, and Air*, 1998, p. V003T08A019.
- [20] Y. Zhao, J. Chi, S. Zhang, and Y. Xiao, "Thermodynamic study of an improved MATIANT cycle with stream split and recompression," *Applied Thermal Engineering*, vol. 125, pp. 452-469, 2017.
- [21] P. Mathieu and R. Nihart, "Sensitivity analysis of the MATIANT cycle," *Energy conversion and management*, vol. 40, pp. 1687-1700, 1999.
- [22] W. Sanz, H. Jericha, F. Luckel, E. Goettlich, and F. Heitmeir, "A further step towards a Graz cycle power plant for CO₂ capture," in *Turbo Expo: Power for Land, Sea, and Air*, 2005, pp. 181-190.
- [23] K. Wimmer and W. Sanz, "Optimization and comparison of the two promising oxy-combustion cycles NET Power cycle and Graz Cycle," *International Journal of Greenhouse Gas Control*, vol. 99, p. 103055, 2020.
- [24] H. Jericha, W. Sanz, and E. Göttlich, "Design concept for large output Graz cycle gas turbines," 2008.
- [25] R. J. Allam, Palmer, M., Brown, G.W, "System and method for high efficiency power generation using a carbon dioxide circulating working fluid," Patent US 2011/0179799A1, 2011.
- [26] R. Allam, S. Martin, B. Forrest, J. Fetvedt, X. Lu, D. Freed, *et al.*, "Demonstration of the Allam Cycle: an update on the development status of a high efficiency supercritical carbon dioxide power process employing full carbon capture," *Energy Procedia*, vol. 114, pp. 5948-5966, 2017.
- [27] M. J. Moran, M. B. Bailey, D. D. Boettner, and H. N. Shapiro, *Fundamentals of engineering thermodynamics*: Wiley, 2018.
- [28] M. J. Moran, H. N. Shapiro, D. D. Boettner, and M. B. Bailey, *Fundamentals of engineering thermodynamics*: John Wiley & Sons, 2010.
- [29] R. Scaccabarozzi, M. Gatti, and E. Martelli, "Thermodynamic analysis and numerical optimization of the NET Power oxy-combustion cycle," *Applied energy*, vol. 178, pp. 505-526, 2016.

- [30] I. Haq and M. Asif, "Energy, exergy and economic analysis of methanol synthesis via coal gasification using solid to liquid concept," *International Journal of Renewable Energy Technology*, vol. 13, pp. 236-264, 2022.
- [31] E. Ersayin and L. Ozgener, "Performance analysis of combined cycle power plants: A case study," *Renewable and Sustainable Energy Reviews*, vol. 43, pp. 832-842, 2015.
- [32] A. Bejan, *Advanced engineering thermodynamics*: John Wiley & Sons, 2016.
- [33] M. Penkuhn and G. Tsatsaronis, "Exergy analysis of the Allam cycle," in *The 5th international symposium–supercritical CO2 power cycles*, 2016, pp. 6-7.
- [34] T. K. Ibrahim, F. Basrawi, O. I. Awad, A. N. Abdullah, G. Najafi, R. Mamat, *et al.*, "Thermal performance of gas turbine power plant based on exergy analysis," *Applied thermal engineering*, vol. 115, pp. 977-985, 2017.
- [35] I. Dincer and M. A. Rosen, *Exergy: energy, environment and sustainable development*: Newnes, 2012.
- [36] L. Barelli, G. Bidini, F. Gallorini, and A. Ottaviano, "An energetic–exergetic comparison between PEMFC and SOFC-based micro-CHP systems," *International Journal of Hydrogen Energy*, vol. 36, pp. 3206-3214, 2011.
- [37] J. Szargut, *Egzergia: poradnik obliczania i stosowania*: Wydawnictwo Politechniki Śląskiej, 2007.
- [38] N. Ferrari, L. Mancuso, J. Davison, P. Chiesa, E. Martelli, and M. C. Romano, "Oxy-turbine for Power Plant with CO2 capture," *Energy Procedia*, vol. 114, pp. 471-480, 2017.
- [39] N. Weiland and D. Thimsen, "A practical look at assumptions and constraints for steady state modeling of sCO2 Brayton power cycles," in *Proceedings of the 5th International Symposium–Supercritical CO2 Power Cycles*, 2016.

DuEPublico

Duisburg-Essen Publications online

UNIVERSITÄT
DUISBURG
ESSEN

Offen im Denken

ub | universitäts
bibliothek

Published in: 6th European Conference on Supercritical CO₂ (sCO₂) for Energy Systems

This text is made available via DuEPublico, the institutional repository of the University of Duisburg-Essen. This version may eventually differ from another version distributed by a commercial publisher.

DOI: 10.17185/duepublico/83301

URN: urn:nbn:de:hbz:465-20250428-124651-1



This work may be used under a Creative Commons Attribution 4.0 License (CC BY 4.0).